Chemical Engineering Science 60 (2005) 565–575

Chemical Engineering Science

www.elsevier.com/locate/ces

Floc model and intrafloc flow

C.P. Chu[a], D.J. Lee[a,*], J.H. Tay[b]

[a]*Chemical Engineering Department, National Taiwan University, 1, Sec. 4 Roosevelt Road, Taipei 10617, Taiwan*
[b]*Division of Environmental and Water Resource Engineering, Nanyang Technological University, Singapore 639798*

Received 24 September 2003; received in revised form 25 July 2004; accepted 25 July 2004
Available online 5 October 2004

Abstract

The three-dimensional pore structures in waste activated sludge floc were identified using the fluorescence in situ hybridization (FISH) and confocal laser scanning microscope (CLSM) images. The meshes of the three-dimensional porous configuration of a sludge floc were constructed from the CLSM series images. The intrafloc flow field was simulated for the constructed floc model when it was subjected to a uniform flow field, based on which the Darcy's permeability was estimated. The permeability (k_{DL}) of original floc was estimated as 8×10^{-12} m^2. Flocculated flocs had higher k_{DL} due to their large pore size, while the corresponding values of k_{DL} of the freeze/thawed flocs were lower. The calculated results indicate that a few large pores in the floc determine the permeability. The fractal dimension and compactness, however, are not correlated with the permeability of the flocs.

Keywords: Structure; Floc model; Pore; CLSM; Transport process

1. Introduction

Flocs generated from biological treatment units are the microreactors that adsorb and decompose pollutants. However, information on the complex geometrical morphology and microbiological ecology inside flocs is still incomprehensive. Moudgil and Shah (1986) stated that the preferred floc properties of different processes were different. Jiwani et al. (1997) monitored several indices of floc morphology (size, compactness, and filament numbers) and correlated then with the quality of the effluent and the dewaterability of the sludge. However, the effects of floc structure, including the spatial distribution of microorganisms, intrinsic mass transfer resistance and possible substrate concentration distribution inside the floc, have not been incorporated into the activated sludge model (Henze et al., 1987; Bakti and Dick, 1992; Keller et al., 2002).

The highly inhomogeneous structure of bioaggregates is difficult to describe using simple geometry. Fractals, whose structures repeat themselves in all dimensions and on all length scales, are often used to characterize the structures of bioaggregates (Mandelbrot, 1983). The fractal dimension D is correlated with the aggregate shape, tortuosity, surface area, and other length-related physical characteristics, defined as,

$$M(R) \propto R^D, \tag{1}$$

where M is the mass and R is the gyration radius. Free-settling tests are widely employed in estimating the fractal dimension of biological flocs (Tambo and Watanabe, 1979; Li and Ganczarczyk, 1989; Lee, 1994). Lee et al. (1996) critically reviewed the use and constraints of the free-settling test. Moreover, light scattering experiments are an important tool for determining the fractal dimension of aggregates. Axford and Herrington (1994), Kyriakidis et al. (1997), Jung et al. (1995), and Guan et al. (1999) use small-angle light scattering to study the structure of flocs. Guan (1999) briefly summarized the limits of the light scattering test.

* Corresponding author. Tel.: +886-22362563200; fax: +886-2-2362-3040.
E-mail address: djlee@ntu.edu.tw (D.J. Lee).

0009-2509/$ - see front matter © 2004 Elsevier Ltd. All rights reserved.
doi:10.1016/j.ces.2004.07.132

Advective flow through the floc dominates the intrafloc transport processes. Adler (1981) determined the streamlines around porous sphere. Wu and Lee (1998) estimated the force exerted on a floc with homogeneous structure moving in an unbounded fluid. They found that higher permeability facilitated flow through the interior of the floc. For a highly porous floc, the flow pattern did not change significantly with the presence of the floc as no boundary layer separation occurred. Wu et al. (1998a,b) and Wu and Lee (1999) simulated the motion of a single sphere moving towards a plate, and recorded the variation of the velocity of a real floc. Permeability was also determined by comparing the experimental data and calculations. A freeze/thawed sludge floc had a more compact structure than the original sludge floc. The terminal velocities of both flocs were higher than that of the solid sphere. The permeability of the activated sludge floc of size 1700–2200 μm ranges 7×10^{-8}–5×10^{-7} m^2.

Bubble-tracing technique visualizes the flow field near the settling floc (Tsou et al., 2002; Wu et al., 2000a,b, 2002; Pietsch et al., 2002). The disturbance by flocs of the paths along which bubbles move can help to estimate the permeability of the flocs. Gorczyca and Ganczarczyk (2001) noted that permeability might not only be a function of floc porosity. Gorczyca and Ganczarczyk (2002) estimated the permeabilities of alum-coagulated flocs and activated sludge flocs by applying the drainage radius model of Adler (1981).

Arguments had arisen concerning the correlation of permeability with porosity, floc size, and floc structure (Gmachowski, 1999; Lee, 1999). Correlations seeking for a simple relationship between permeability and floc properties faced difficulty by neglecting the complex nature of the floc interior. In this study, the three-dimensional configuration of the porous interior of a sludge floc was constructed using the confocal laser scanning microscope (CLSM) series images. The flow field in the floc interior was simulated based on which the relationship between average fluid flow rate and the applied pressure drop was estimated. Comments on the correlations between floc permeability and interior geometric parameters were given.

Jorand et al. (1995) measured the change in floc size after ultrasonication and showed that a single floc (125 μm) consists of many small aggregates (approximately 13 μm), and these aggregates are composed of bacteria cells of approximately 2.5 μm. Sanin and Vesilind (1996) first combined the aforementioned information to simulate a floc. In the pertinent literature, Lee (1999) appeared as the first author who proposed the fractal-of-fractals structure of biological flocs. Following Lee's proposal, Wu et al. (2002) experimentally revealed that the fractal dimensions of a sludge sample probed using free-settling test and small-angle light scattering test are not identical. Most analyses of fluid dynamics and mass transfer generally assume that the floc interior is uniform for simplicity (Wu and Lee, 1998a,b, 1999, 2001; Tsou et al., 2002), and they neglect the determinative effect of the floc structure.

We detailed the floc's interior structure by employing the fluorescence in situ hybridization (FISH) and CLSM, and subsequently, established the three-dimensional floc model. The flow field in the floc interior was simulated based on which the relationship between average fluid flow rate and the applied pressure drop was estimated. The correlations between floc permeability and interior geometric parameters were commented.

2. Establishing floc model

2.1. The sample and tests

Waste activated sludge was taken from the Min-Sheng Municipal Wastewater Treatment Plant in Taipei, which was gravitationally settled to a solid content of 15,000 mg/L, and was the testing sample for the present test. The pH value of the sludge was approximately 6.2. The chemical oxygen demand (COD) for the sludge was 24,400 mg/L, obtained from direct reading spectrometer (DR/2000, HACH, USA). The COD for the filtrate of sludge sample after filtering through a 0.45 μm membrane was termed as soluble COD (SCOD), which read 510 mg/L for the original sludge. The elemental compositions of dried sample were C: 34.3%, H: 5.5%, and N: 5.5%, using elemental analyzer (Perkin-Elmer 2400 CHN). Dry solids density of sludge was measured by an Accupyc Pycnometer 1330 (Micromeritics) as 1450 kg/m^3.

The cationic flocculant, a polyacrylamide indicated as polymer T-3052, was obtained from Kai-Guan Inc., Taiwan. The polymer T-3052 has an average molecular weight of 10^7 daltons (Da) and a charge density of 20%. The polymer solution was gradually poured into the mixing vessel containing fresh sludge samples with 200 rpm of stirring for 5 min (rapid mix) followed by 50 rpm of another 20 min (slow mix) (Chang et al., 1997). Based on filterability tests (data not shown), the "optimal" dose of polyelectrolyte for the present sludge was noted 40 ppm, and was used as the dose adopted herein.

Freezing and thawing tests were conducted in an air-cooling room of −17 °C. The sludge sample was placed in a container of diameter 3.5 cm and height 3 cm. Complete freezing was achieved in 2 h of freezing. The frozen sample was then cured at the same subfreezing temperature for another 22 h. After freezing the sample was thawed at room temperature for 6 h (Hung et al., 1996).

The present work employed the CLSM (OLYMPUS BX50) equipped with an image processor (OLYMPUS FV5 PSU) and an argon laser source to stimulate the fluorescence. The sludge floc was imaged with a 10× objective with the software FLUOVIEW version 3.0. A microscope scanned the samples at fixed depth and digitized the image obtained. Sludge flocs for CLSM analysis were first fixed with 3% paraformadehyde in phosphate-buffered saline (PBS). Then the fixed sample was embedded in low-melting-point agar (with melting point of 75 °C and gelling point of 38 °C) for the FISH. In this study, we used the

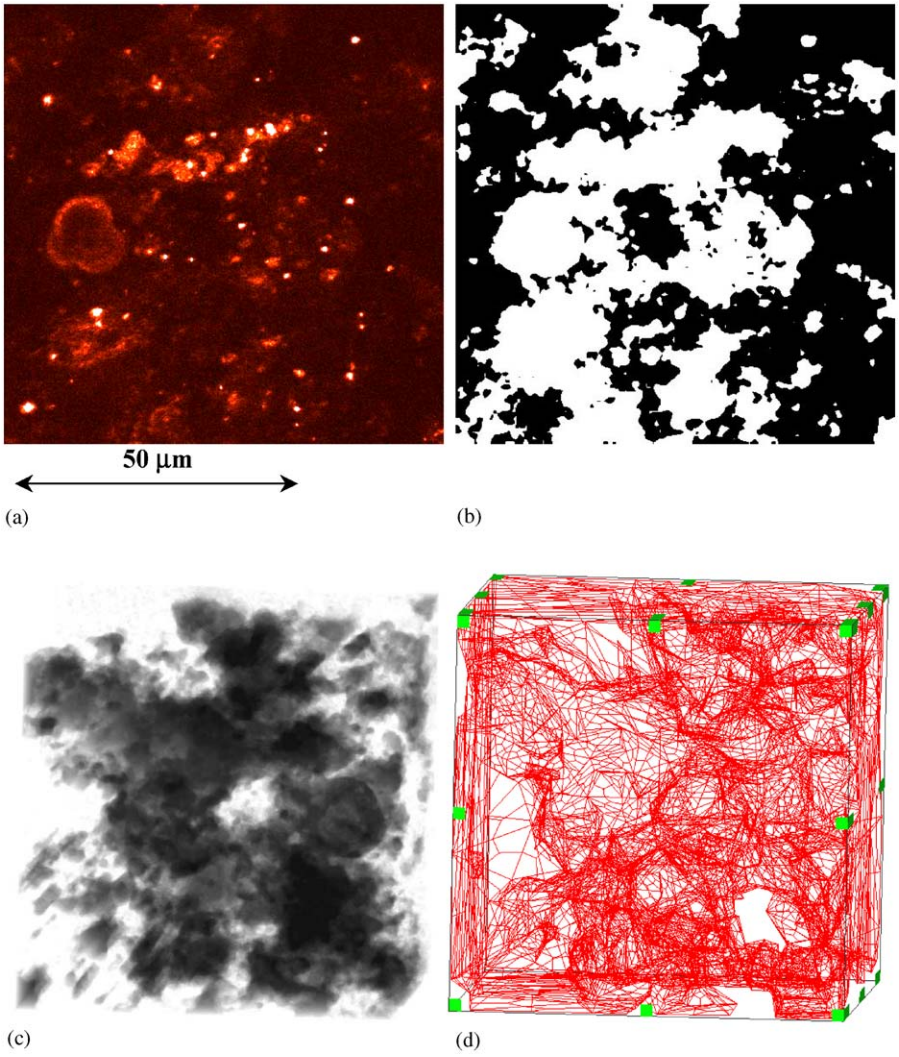

Fig. 1. Original floc: ID #C. (a) Typical CLSM sliced image; (b) bilevel image (thresholded by Otsu's method); (c) three-dimensional view of floc biomass; (d) hexahedral volumetric grids of the pore.

probe, EUB338 (labeled by rhodamine) and ARCH915 (labeled by tetrachlorofluorescein), for detection of members of domain Bacteria with high cellular ribosome content and those that cannot be detected by EUB338. The stained samples were washed three times to remove extra probes by hybridization buffer solution.

2.2. Floc model

More than 150 CLSM images were sampled for a typical floc, and the image-thresholding algorithm—Otsu's method (Pietsch et al., 2002)—determined the thresholding values of sliced images. A region of interest (ROI) was selected for bileveling process. Afterwards, the three-dimensional image for the floc was reconstructed using the bileveled CLSM images. Then, the software, *Amira* 3.0 (TGS Inc., USA), was used to reconstruct the thresholded sliced images as isosurfaces (polygonal surface models and volumetric grids) with the procedure as follows:

(1) To reduce the resolution of the image and adjust the physical shape of the voxel to almost a cube. In this study, the typical resolutions of the sliced images in the X and Y directions are about 0.2 μm/pixel (100 μm/512 pixels), and the physical interval between the two CLSM slices is approximately 1 μm. Herein, the sliced image resolution was reduced from 512×512 to 128×128 (image resampling) so the ratio X:Y:Z of the voxel was all about unity. The Lanczos filter is used in the resampling.

(2) To detect the edges in the bilevel images. Boundaries in the binary images are classified according to connectivity and whether they lie within the object or its complement. The connectivity of neighboring pixels in all analyses is set to four for edge detection.

(3) To establish the three-dimensional shape of the object. When the boundaries have been sketched, the isosurfaces can

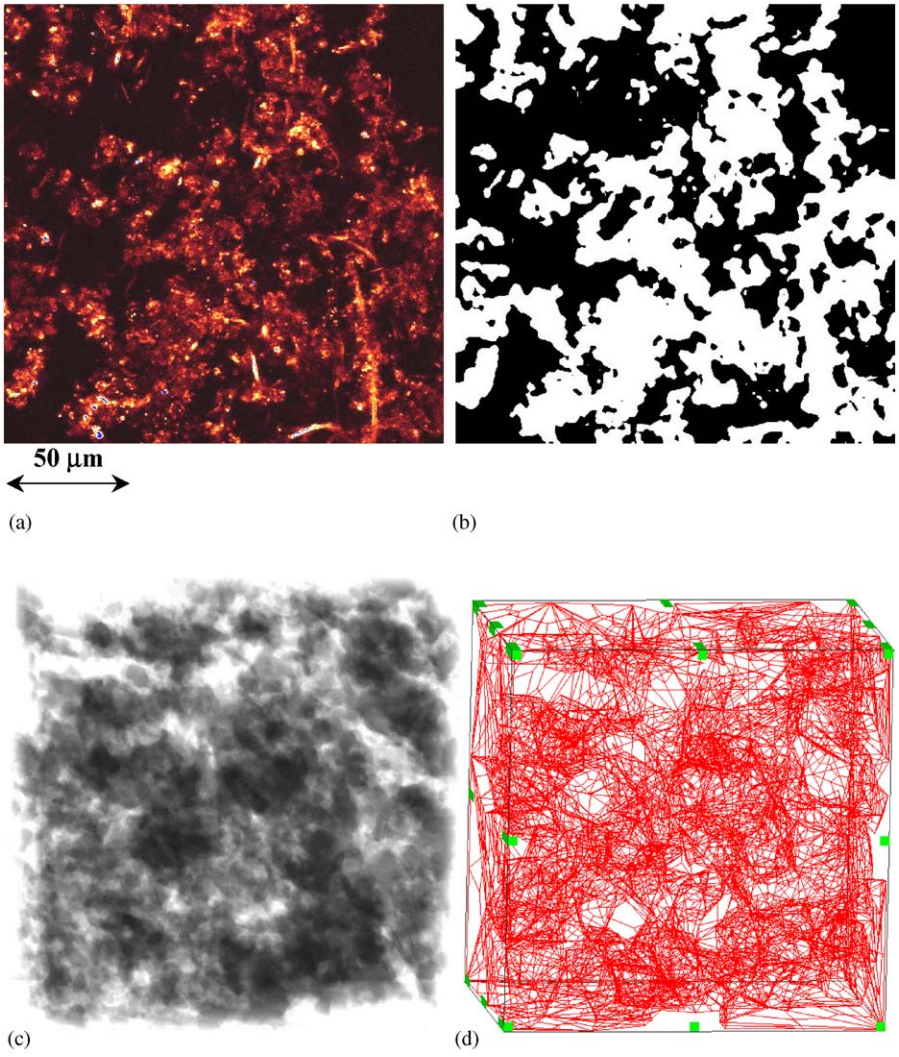

Fig. 2. Cationically flocculated floc: ID #C. (a) Typical CLSM sliced image; (b) bilevel image (thresholded by Otsu's method); (c) three-dimensional view of floc biomass; (d) hexahedral volumetric grids of the pore.

be established to demonstrate the three-dimensional shape of the object. The surface construction algorithm adopted here is the *marching cubes* algorithm for triangulating surfaces (Lorensen and Cline, 1987).

(4) The *advancing-front algorithm* is applied to fill each region defined by the simplified polygonal surface model of pores, with unstructured tetrahedral volumetric grids (Chu and Lee, 2004). The tetrahedral grids were converted to equivalent hexahedral grids to be compactible for the fluid dynamic software. Each tetrahedral grid was converted to four hexahedral grids.

According to the procedures described in the preceding section, the typical CLSM sliced image, the bileveled image, the three-dimensional reconstructed image for biomass, and the established grids for void space were demonstrated for the original sludge floc (Fig. 1), the cationically flocculated floc (Fig. 2), and freeze/thawed sludge floc (Fig. 3). Table 1 presents the length (X), width (Y) and height (Z) of a cuboid model. A total of nine flocs were examined in this work.

The compactness of a three-dimensional object is defined as $A^3/36\pi V^2$, where A and V are the surface area and volume of the biomass phase, respectively. The compactness of a sphere equals one. The original sludge flocs had compactness between 30 and 50 (Table 1), whereas the compactness of flocculated sludge flocs was extremely high (200–1300). In contrast, the compactness of the freeze/thawed flocs is relatively low (19–33), implying that the flocs were more spherical shape than the other samples.

The box-counting fractal dimension $D_{P,3}$ is given by Eq. (2), if the surface of one fractal object is covered by triangular patches with a characteristic side length, l_{equi}, (Baveye et al., 1998);

$$D_{P,3} = -\lim_{l_{\text{equi}} \to 0} \frac{\log n(l_{\text{equi}})}{\log l_{\text{equi}}}, \tag{2}$$

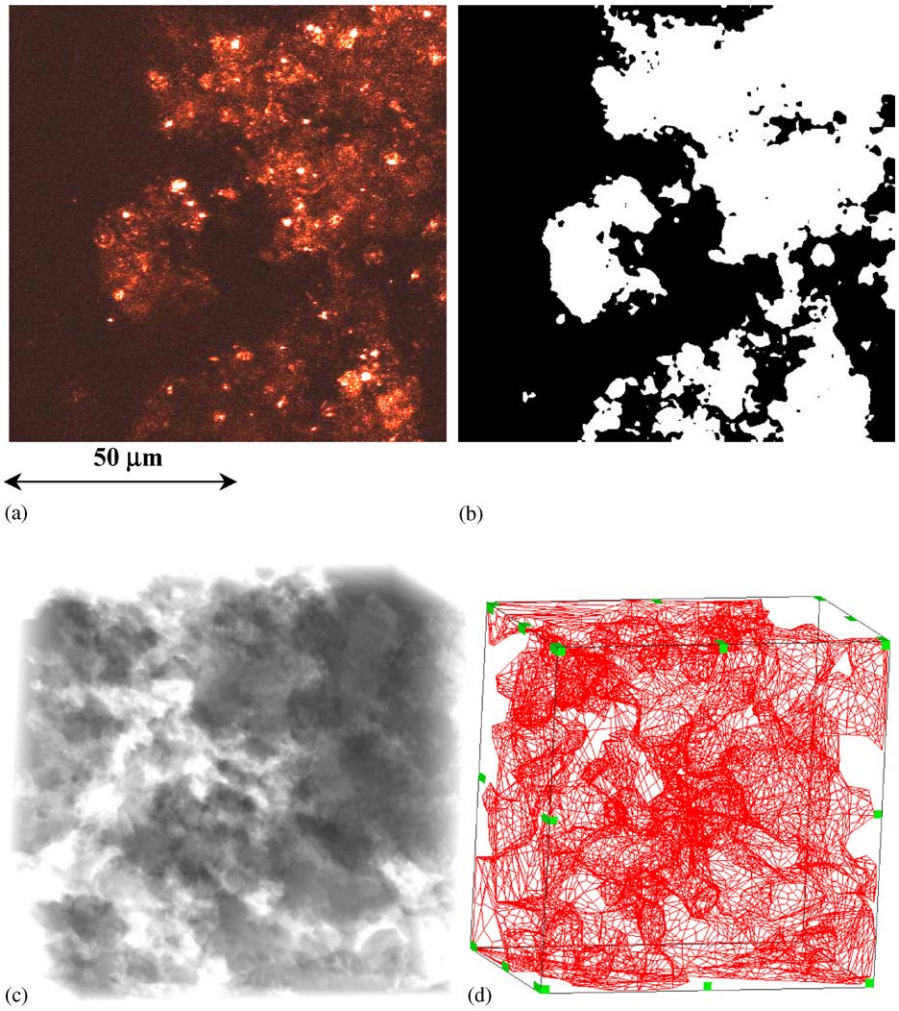

Fig. 3. Freeze/thawed floc: ID #C. (a) Typical CLSM sliced image; (b) bilevel image (thresholded by Otsu's method); (c) three-dimensional view of floc biomass; (d) hexahedral volumetric grids of the pore.

Table 1
The tortuosity and permeability of the original, cationic flocculated, and freeze/thawed flocs

Floc ID	Size (μm × μm × μm)	$D_{P,3}$	Compactness	τ	$k_{DL,X}$ (m^2)	$k_{DL,Y}$ (m^2)	$k_{DL,Z}$ (m^2)	k_{DL} (m^2)
Original floc								
A	$113 \times 113 \times 102$	2.56	51	1.44	7.1×10^{-12}	7.7×10^{-12}	9.0×10^{-12}	7.9×10^{-12}
B	$93.8 \times 93.8 \times 74.9$	2.57	38	1.28	6.1×10^{-12}	1.0×10^{-11}	7.4×10^{-12}	7.7×10^{-12}
C	$77.7 \times 77.7 \times 112$	2.58	32	1.48	7.6×10^{-12}	5.3×10^{-12}	1.0×10^{-11}	7.5×10^{-12}
Cationically flocculated floc								
A	$238 \times 238 \times 198$	2.70	1,300	1.38	4.5×10^{-11}	3.3×10^{-11}	8.0×10^{-11}	4.9×10^{-11}
B	$188 \times 188 \times 132$	2.63	210	1.58	9.9×10^{-12}	8.8×10^{-12}	1.4×10^{-11}	1.1×10^{-11}
C	$178 \times 178 \times 134$	2.62	410	1.32	2.3×10^{-11}	2.6×10^{-11}	3.5×10^{-11}	2.7×10^{-11}
Freeze/thawed floc								
A	$122 \times 122 \times 88.2$	2.46	25	1.26	1.9×10^{-11}	3.9×10^{-11}	1.8×10^{-11}	2.3×10^{-11}
B	$93.8 \times 93.8 \times 51.0$	2.46	19	1.39	7.4×10^{-12}	6.5×10^{-12}	6.7×10^{-12}	6.8×10^{-12}
C	$93.8 \times 93.8 \times 59.1$	2.51	34	1.31	5.8×10^{-12}	7.1×10^{-12}	4.1×10^{-12}	5.5×10^{-12}

where $n(l_{\text{equi}})$ is the number of triangular patches. In practice, the limit $l_{\text{equi}} \to 0$ cannot be approached. $D_{P,3}$ is estimated by measuring the dependence of n on l_{equi} when the characteristic length is larger than some cut-off length, which is the size in pixels of the original sliced image. The original sludge flocs had $D_{P,3}$ of about 2.57. The cationic flocculated sludge flocs with more irregular surfaces had the higher $D_{P,3}$ (2.62–2.70), and freeze/thawed sludge flocs had lower $D_{P,3}$ (2.45–2.50) than the original flocs (Table 1).

3. Intrafloc transport

3.1. Equations and solution

The models depicted in Figs. 1–3 can be used to simulate the intrafloc advective flow, and subsequently to estimate the effective permeability of the sludge floc. The shape of model is roughly a cuboid. One of the six faces on the cuboid model was defined as the inlet, and the opposite face was defined as the outlet. Thus, every cuboid model has three cases for calculations—*X*, *Y* and *Z* directions, as shown in Fig. 4. This model floc was placed at the center of a fluid field of width and length 15 and 75 times to the floc model (Fig. 5). A uniform fluid flow U was imposed at the entry plane and at the side-wall. This flow system is equivalent to that with a model floc moving at a velocity U though an unbound, quiescent water pool. The direction of U is set as parallel to the *X*, *Y* or *Z*-axis, respectively, for exploring the effective permeability along each principal direction. The governing equations of the fluid flow are stated as follows:

$$\left(\vec{u}^{\,*} \bullet \nabla^*\right) \vec{u}^{\,*} + \left(\frac{P_0}{\rho U^2}\right) \nabla^* P^* = \frac{\mu}{\rho U d_f} \nabla^{*2} \vec{u}^{\,*}, \quad (3)$$

$$\vec{u}^{\,*} = \vec{U}^{\,*} \mathrm{i} \quad \text{at inlet plane and outside fluid wall} \quad (4a)$$

$$\vec{u}^{\,*} = \vec{0} \quad \text{at solids surface,} \quad (4b)$$

where u is the fluid velocity, P_0 is the pressure at the inlet plane, d_f is defined as the geometric mean of the length, width and height in Table 1

$$\left(\sqrt[3]{L_X L_Y L_Z}\right), \quad \vec{u}^{\,*} = \frac{\vec{u}}{U}, \quad \text{and} \quad \nabla^* = \frac{\nabla}{d_f}.$$

The hexahedral grids generated using *Amira* 3.0 were first preprocessed using geometry modeling/mesh generation software, GAMBIT 2.0 (Fluent Inc., USA), to define the inlet, outlet and walls, to solve the governing Eq. (3), subject to the associated boundary conditions Eqs. (4a) and (4b). The models were then solved using software, FLUENT 6.0 (Fluent Inc., USA). The pressure–velocity coupling algorithm was SIMPLEC (Semi-Implicit Method for Pressure-Linked Equations-Consistent). The calculation was performed at a maximum relative error of 0.1%.

3.2. Intrafloc advective flow

The intrafloc flow pattern was displayed using a plot of the path lines. The trajectory function was defined as,

$$\frac{\mathrm{d}x}{\mathrm{d}t} = u_{p,X}(x, y, z, t) \quad (5a)$$

$$\frac{\mathrm{d}y}{\mathrm{d}t} = u_{p,Y}(x, y, z, t) \quad (5b)$$

$$\frac{\mathrm{d}z}{\mathrm{d}t} = u_{p,Z}(x, y, z, t) \quad (5c)$$

The particles are initially released from the inlet and finally arrived at the outlet under normal conditions. Figs. 6a–c plot the path lines of the *X*-directional flow for original, flocculated, and freeze/thawed flocs (#C). The maximum number of steps by which a particle can advance is set to 1000. Path lines were colored according to the static pressure (gauge), measured in pascals. Note that the sizes of the flocculated flocs are larger than the original or the freeze/thawed flocs. Hence, it is evident that the local intrafloc advective flow is stronger for the former than for the latter two. This occurrence is attributable to the fact that the flocculation would produce larger internal pores.

The path lines in Figs. 6a–c estimate the tortuosity of the tunnels in the floc. The path length of all lines in three directions was averaged, and the average was determined and divided by the geometric mean of cuboids. This ratio was defined as the average tortuosity τ and listed in Table 1. The tortuosity ranged from 1.25 to 1.60. Although the values of τ did not vary greatly among in the nine cases, the flocculated sludge flocs had a slightly higher tortuosity than the other two types of flocs.

The area-weighted average pressure of the cross sections perpendicular to the flow direction was used to determine the average pressure drop in the floc, and the permeability, based on Darcy's law, was estimated. Figs. 7–9 plot the pressure drop, and Table 1 lists the calculated permeabilities. Three observations are made:

(1) The pressure drops over the flocculated flocs are much lower than those over the original or freeze/thawed flocs, although the floc sizes for the former are greater. Chung et al. (2003) estimated the drag force exerted on sludge flocs over Reynolds number of 11–26, leading to an average drag force gradient at 0.5–3.0 $\times 10^{-4}$ N/m of floc length. With the floc size the calculated pressure drop data presented in Fig. 7, a fairly comparable drag force gradient is estimated: around 10^{-4} N/m of floc length for the present calculated cases.

(2) The order of magnitude of floc permeability estimated using the cuboid models is 10^{-12}–10^{-10} m^2. This value is much lower than the values of k_{DL} for the straight tunnels in a sphere of similar porosity (roughly 6×10^{-9} m^2 as shown in an independent calculation), and the experimental values reported by Tsou et al. (2002) (ranging from 10^{-9} to 10^{-7} m^2). The former discrepancy demonstrated the

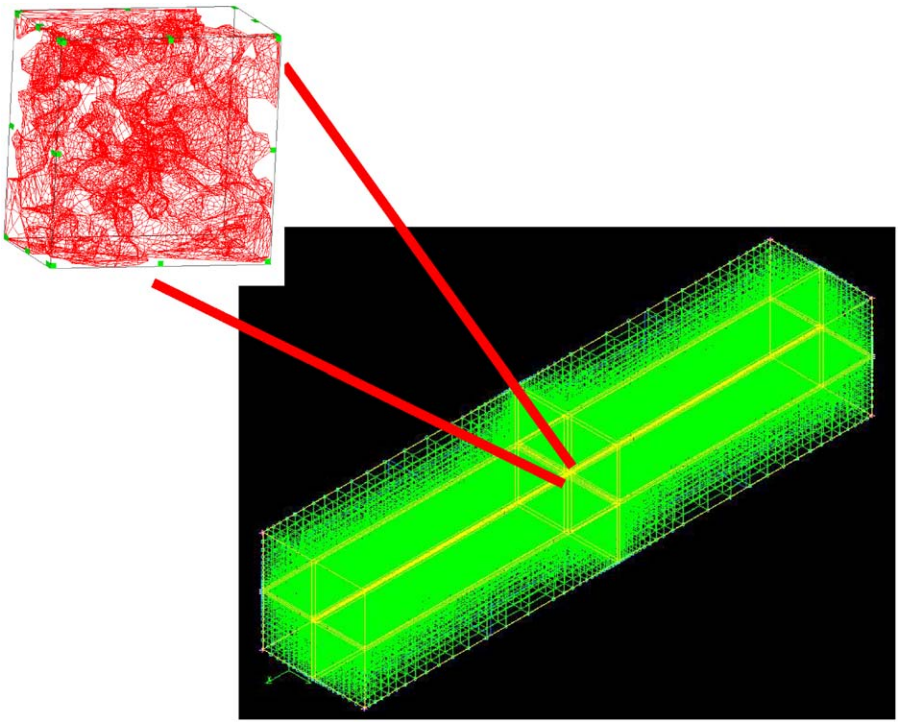

Fig. 4. Computational domain for the fluid flow field around and through the floc.

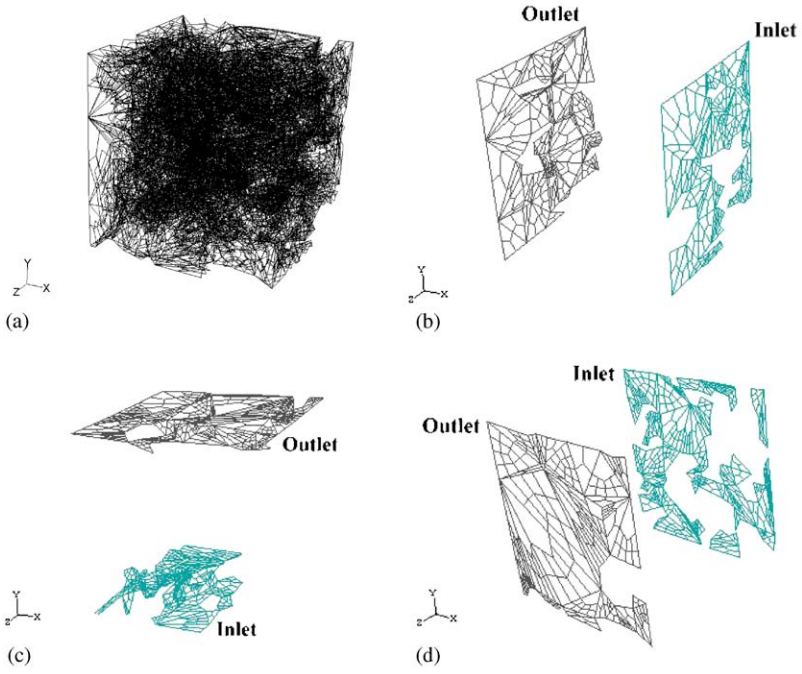

Fig. 5. An example of cuboid model (original floc): (a) the entire meshes; (b) inlet and out in the direction *X*; (c) inlet and out in the direction *Y*; (d) inlet and out in the direction *Z*.

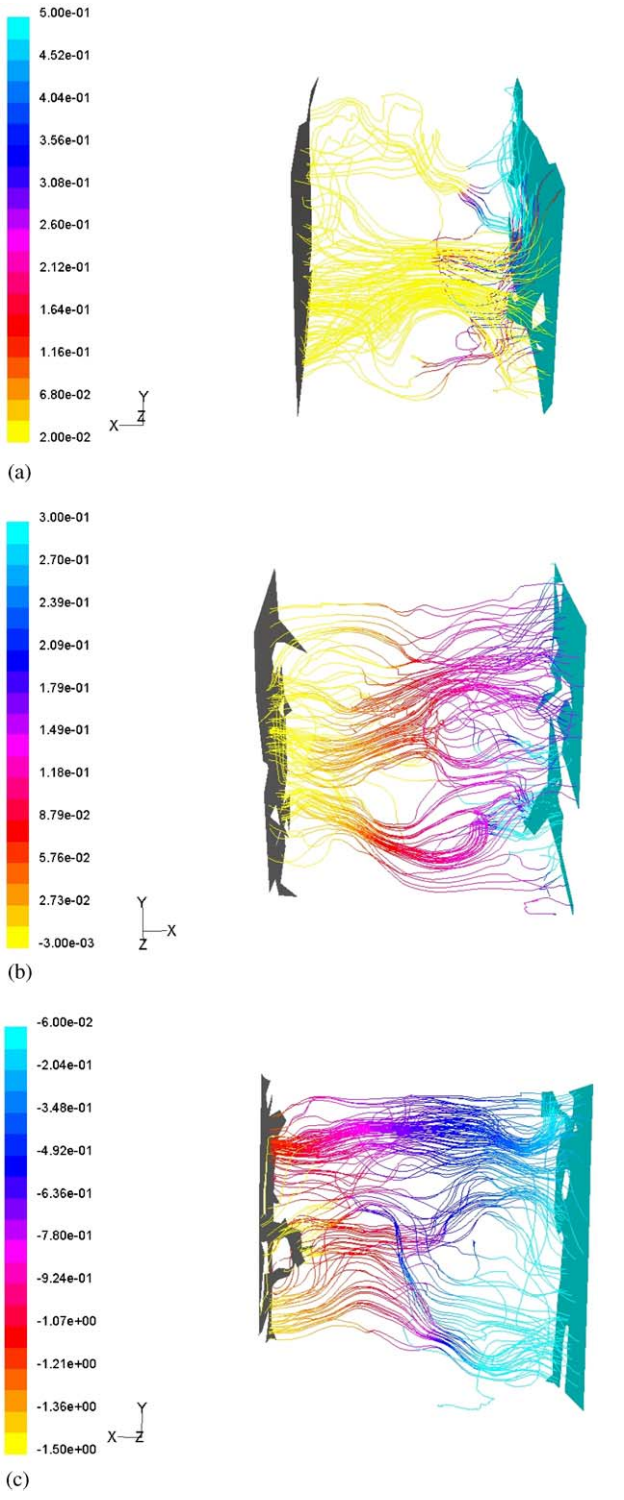

Fig. 6. (a) Path lines plot of original floc C (*X*-direction); colored by static pressure (pa, gauge). (b) Path lines plot of cationically flocculated floc C (*X*-direction); colored by static pressure (pa, gauge). (c) Path lines plot of freeze/thawed floc C (*X*-direction); colored by static pressure (pa, gauge).

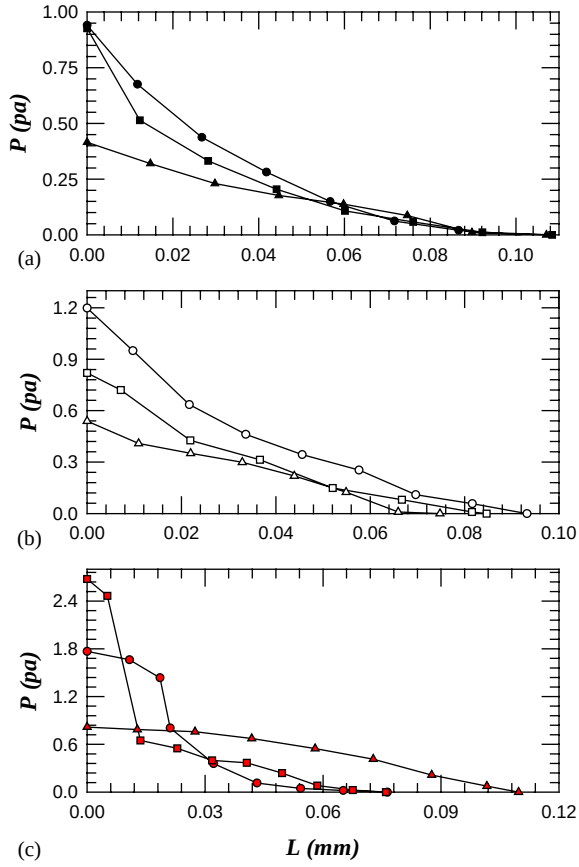

Fig. 7. Pressure drop in the cuboid model of original flocs: (a) floc A; (b) floc B; (c) floc C. (Circles: *X*-direction; Squares: *Y*-direction; Triangles: *Z*-direction).

importance of the pore tortuosity on the permeability. The discrepancy with the measurement by Tsou et al. could be explained by the possible size effect. The flocs examined by Tsou et al. were in size of 1700–2200 μm, for easy measurement of the stick deformation with the floc subjected to a crossflow. The original flocs in the present work have a size of 78–113 μm, better representing the typical flocs noted in the aeration basin. Restated, the flocs examined in Tsou et al. were almost 20–60 times larger than the flocs studied herein. As known for the fractal-like objects, the effective permeability increases nearly with the square of the floc size (which is nearly proportional to the cross-sectional area of the largest pore in the floc). Hence, the permeability data presented in this work would be only $\frac{1}{400}-\frac{1}{3600}$ to Tsou et al., if the fractal structure of the two batches of flocs were similar.

(3) Comparing the permeabilities in the *X*, *Y* and *Z* directions reveals that the three values are not the same. The highly heterogeneous distribution of biomass in the floc caused the configuration in the three directions to be anisotropic. Zartarian et al. (1997) also reported this anisotropic growth in the floc, determined from the calculation of local curvatures. The mean permeability k_{DL} of the floc was thus defined as the geometric mean of three permeabilities $\left(\sqrt[3]{k_{DL,X}k_{DL,Y}k_{DL,Z}}\right)$. The average permeability of the three original sludge flocs is approximately

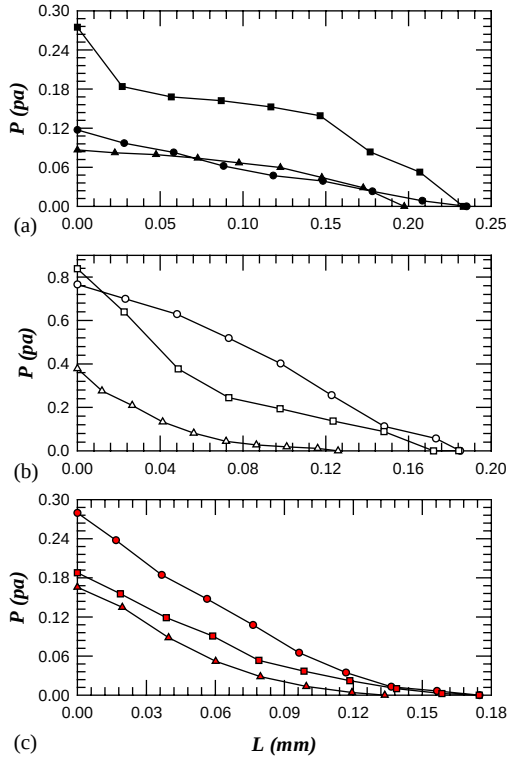

Fig. 8. Pressure drop in the cuboid model of cationically flocculated flocs: (a) floc A; (b) floc B; (c) floc C. (Circles: *X*-direction; Squares: *Y*-direction; Triangles: *Z*-direction).

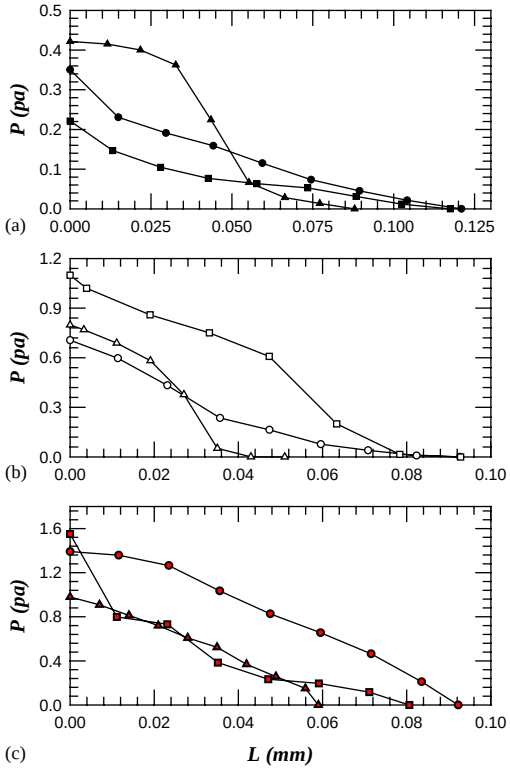

Fig. 9. Pressure drop in the cuboid model of freeze/thawed flocs: (a) floc A; (b) floc B; (c) floc C. (Circles: *X*-direction; Squares: *Y*-direction; Triangles: *Z*-direction).

$8 \times 10^{-12}\,\mathrm{m}^2$. The flocculated sludge flocs have a permeability ($1.0–4.9 \times 10^{-11}\,\mathrm{m}^2$) of approximately three times that of the original samples. Larger interstices promote flow and lead to a higher permeability. The freeze/thawed sludge floc B and C had the lowest permeability of the three types of flocs ($6 \times 10^{-12}\,\mathrm{m}^2$). Their much more compact structure increases the flow resistance, reducing k_{DL}. The freeze/thawed floc A had a relatively high permeability, possibly because its biomass was distributed along the diagonal lines of the cuboid model rather than uniformly occupying the space. Although the permeability reported herein is much lower than the experimental value (Tsou et al., 2002) owing to the different size range under investigation, the order of relative magnitudes is the same-flocculated flocs > original samples > freeze/thawed samples.

Although the rugged surface produces more friction during motion than a smooth surface, flocs with higher compactness or fractal dimension $D_{P,3}$ are not always less permeable. For example, although original floc A had much higher compactness (51) than the other two flocs (38 and 32), it remained the most permeable. Furthermore, although the cuboid model of the flocculated sludge flocs had more rugged pore surfaces (higher $D_{P,3}$ and compactness) than those of the original flocs, the flocculated flocs was clearly the most permeable. The results in Table 1 indicate that the pore size and tortuosity more affected the permeability than did the compactness and fractal dimensions. Generally, larger pores and a lower average tortuosity favor for passing of fluid and a high permeability. The moisture tends to flow along the path, through the floc interior of the least resistance, so only a few large pores (interstices) contribute most permeability. Fig. 10 plots the accumulated fraction of flow rate against the accumulated area fraction of porous regions on the cross section (A/A_{total}), where A is calculated starting from the largest pores and downward, and Q is the corresponding accumulated flow rate. For all the cases, 90% of fluid passed through the interstices whose area was less than 50% of the area of the entire porous regions. The commonly adopted permeability model, assuming a homogeneous interior, may be misused to estimate the permeability of a sludge floc with highly heterogeneous structure.

In contrast, the effects of fractal dimension on the flow pattern are not important as expected, quite straightforwardly because the fractal geometry is expressed in the self-similarity between the large scale (the whole flocs) and the small scale (primary aggregates). Restated, since most structural details, such as studs or pores, contribute negligibly to permeability, this attribute is not influenced by the fractal dimension or compactness. The detailed pore structure, however, should have affected the transport processes near the biomass surface, determined mainly by molecular diffusion and surface adsorption.

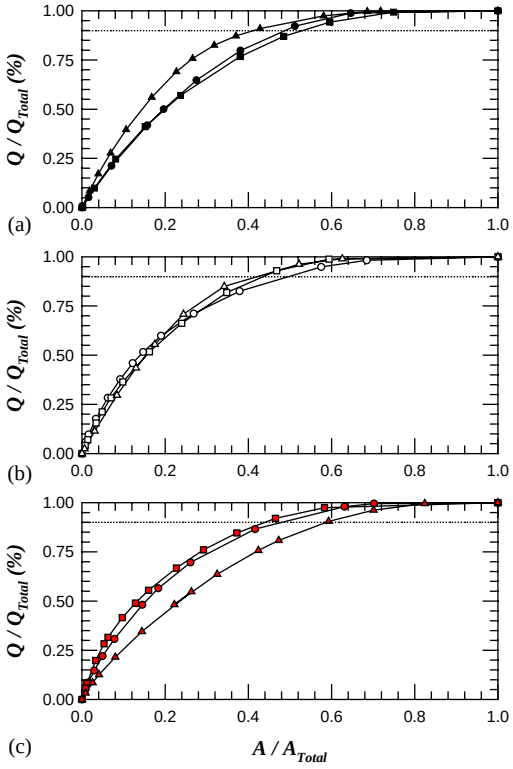

Fig. 10. The accumulated fraction of flow rate against the area fraction of porous regions on the cross section of Figs. 1–3: (a) original flocs; (b) cationically flocculated flocs; (c) freeze/thawed flocs (circles: floc A; squares: floc B; triangles: floc C).

4. Conclusions

This work probed the three-dimensional structure of flocs using the FISH and the CLSM. The CLSM images for sludge floc, original, cationically flocculated, or freeze/thawed, were sampled, bileveled, and used to construct the polygonal surface models and volumetric grids. The floc interior was highly heterogeneous, while the flocculation produced long pores with rugged pore surface, and the freezing and thawing yielded short pores with smooth pore surface. The intrafloc fluid field subjected to a uniform flow was numerically evaluated based on the constructed floc models. The calculated pressure drops over the flocculated flocs are much lower than those over the original or freeze/thawed flocs, although the floc sizes for the former are greater. This result corresponded to the drag force exerted on sludge floc, as Chung et al. (2003) reported. Meanwhile, the order of magnitude of floc permeability estimated using the cuboid models is 10^{-12}–10^{-10} m^2 for floc of size 78–113 μm. The permeability follows the order: flocculated flocs > original samples > freeze/thawed samples. Ninety percent of fluid passed through the interstices whose area was less than 50% of the area of the entire porous regions. In contrast, the effects of fractal dimension on the flow pattern are not important.

References

Adler, P.M., 1981. Streamlines in and around porous particles. Journal of Colloid and Interface Science 81, 531–535.

Axford, S.D.T., Herrington, T.M., 1994. Determination of aggregate structures by combined light-scattering and rheological studies. Journal of the Chemical Society-Faraday Transactions 90, 2085–2093.

Bakti, N.A.K., Dick, R.I., 1992. A model for a nitrifying suspended-growth reactor incorporating interparticle diffusional limitation. Water Research 26, 1681–1690.

Baveye, P., Boast, C.W., Ogawa, S., Parlange, J.-Y., Steenhuis, T., 1998. Influence of image resolution and thresholding on the apparent mass fractal characteristics of preferential flow patterns in field soils. Water Resource Research 34 (11), 2783–2796.

Chang, I.L., Chu, C.P., Lee, D.J., Huang, C.P., 1997. Effects of polymer dose on filtration followed by expression characteristics of clay slurries. Journal of Colloid and Interface Science 185, 335–342.

Chu, C.P., Lee, D.J., 2004. Multiscale structures of biological flocs. Chemical Engineering Science 59, 1875–1883.

Chung, H.Y., Ju, S.P., Lee, D.J., 2003. Hydrodynamic drag force exerted on waste activated sludge floc. Journal of Colloid and Interface Science 263, 498–505.

Gorczyca, B., Ganczarczyk, J.J., 2001. Fractal analysis of pore distributions in alum coagulation and activated sludge flocs. Water Pollution Research Journal of Canada 36, 687–700.

Gorczyca, B., Ganczarczyk, J.J., 2002. Flow rates through alum coagulation and activated sludge flocs. Water Pollution Research Journal of Canada 37, 389–398.

Guan, J., 1999. Implications of floc structure to solid–liquid separation processes in wastewater treatment. Ph.D. Thesis, School of Civil and Environmental Engineering, University of New South Wales, Sydney, Australia.

Guan, J., Waite, T.D., Amal, R., 1999. Rapid structure characterization of bacterial aggregates. Environmental Science and Technology 32, 3735–3742.

Henze, M., Grady, C.P.L., Gruyer, W., Marais, G.V.R., Matsuo, T., 1987. A general model for single sludge wastewater treatment systems. Water Research 21, 505–515.

Hung, W.T., Chang, I.L., Lin, W.W., Lee, D.J., 1996. Unidirectional freezing of waste activated sludge: effects of freezing speed. Environmental Science and Technology 30, 2391–2396.

Jiwani, A., Graham, N.J.D., Day, M.C., 1997. Activated sludge process control via particle monitoring. Water Science and Technology 36 (4), 269–277.

Jorand, F., Zartarian, F., Thomas, F., Block, J.C., Bottero, J.Y., Villemin, G., Urbain, V., Manem, J., 1995. Chemical and structural (2D) linkage between bacteria within activated sludge flocs. Water Research 29, 1639–1647.

Jung, S.J., Amal, R., Raper, J.A., 1995. Use of small angle light scattering to study structure of flocs. Particle and Particle System Characterization 12, 274–278.

Keller, J., Yuan, Z., Blackall, L.L., 2002. Integrating process engineering and microbiology tools to advance activated sludge wastewater treatment research and development. Reviews in Environmental Science and Biotechnology 1, 83–87.

Kyriakidis, A.S., Yiantsios, S.G., Karabelas, A.J., 1997. A study of colloidal particle Brownian aggregation by light scattering techniques. Journal of Colloid and Interface Science 195, 299–306.

Lee, D.J., 1994. Floc structure and bound water content in excess activated sludges. Journal of Chinese Institute of Chemical Engineers 25, 201–207.

Lee, D.J., 1999. Reply to comment by L. Gmachowski. Water Research 33, 1116.

Lee, D.J., Chen, G.W., Liao, Y.C., Hsieh, C.C., 1996. On the free settling tests for estimating activated sludge floc density. Water Research 30, 541–550.

Li, D.H., Ganczarczyk, J.J., 1989. Fractal geometry of particle aggregates generated in water and wastewater treatment processes. Environmental Science and Technology 23, 1385–1389.

Lorensen, W.E., Cline, H.E., 1987. Marching cubes: a high resolution 3D surface construction algorithm. Computer Graphics 21, 163–169.

Mandelbrot, B.B., 1983. The Fractal Geometry of Nature, W. H. Freeman and Co., New York.

Moudgil, B.M., Shah, B.D., 1986. Selection of flocculants for solid–liquid separation processes. In: Muralidhara, H.S. (Ed.), Advances in Solid–Liquid Separation. Battelle Press, Columbus, OH, USA.

Pietsch, T., Mehrwald, R., Grajetzki, R., Sens, J., Pakendorf, T., Ulrich, R., Kumpart, J., Matz, G., Märkl, H., 2002. Macro- and microscopic in-situ observation of gas bubbles and sludge particles in a biogas tower reactor. Water Research 36, 2836–2842.

Sanin, F.D., Vesilind, P.A., 1996. Synthetic sludge: a physical/chemical model in understanding bioflocculation. Water Environment Research 68, 927–933.

Tambo, N., Watanabe, Y., 1979. Physical characteristics of floc—I. The floc density function and aluminum floc. Water Research 13, 409–419.

Tsou, G.W., Wu, R.M., Yen, P.S., Lee, D.J., Peng, X.F., 2002. Advective flow and floc permeability. Journal of Colloid and Interface Science 250, 400–408.

Wu, R.M., Lee, D.J., 1998a. Hydrodynamic drag force exerted on a moving floc and its implications to free settling test. Water Research 32, 860–868.

Wu, R.M., Lee, D.J., 1998b. Hydrodynamic drag force exerted on a highly porous sphere moving towards an impermeable plate. Chemical Engineering Science 53, 3571–3578.

Wu, R.M., Lee, D.J., 1999. Highly porous sphere moving through centerline of circular tube filled with Newtonian fluid. Chemical Engineering Science 54, 5717–5724.

Wu, R.M., Lee, D.J., 2001. Hydrodynamic drag on non-spherical floc and free-settling test. Water Research 35, 3226–3234.

Wu, R.M., Tsou, G.W., Lee, D.J., 2000a. Estimation of the interior permeability of polymer-flocculated sludge flocs. Advances in Environmental Research 4, 163–167.

Wu, R.M., Tsou, G.W., Lee, D.J., 2000b. Estimate of sludge floc permeability. Chemical Engineering Journal 80, 37–42.

Wu, R.M., Lee, D.J., Waite, T.D., Guan, J., 2002. Multilevel structure of sludge flocs. Journal of Colloid and Interface Science 252, 383–392.

Zartarian, F., Mustin, C., Villemin, G., Ait-Ettager, T., Thill, A., Bottero, J.Y., Mallet, J.L., Snidaro, D., 1997. Three-dimensional modeling of an activated sludge floc. Langmuir 13, 35–40.